J Solid State Electrochem (2007) 11:571–576
DOI 10.1007/s10008-006-0197-9

ORIGINAL PAPER

Nanocrystalline nickel cobalt hydroxides/ultrastable Y zeolite composite for electrochemical capacitors

Yan-Yu Liang · Shu-Juan Bao · Hu-Lin Li

Received: 8 March 2006 / Revised: 27 June 2006 / Accepted: 2 July 2006 / Published online: 5 September 2006

Abstract A novel nanocomposite of $Co(OH)_2$–$Ni(OH)_2$ and ultrastable Y molecular sieves was synthesized by an improved chemical precipitation method for electrochemical capacitors. The $Co(OH)_2$–$Ni(OH)_2$/ultrastable Y zeolite (USY) composite and its microstructure were characterized by scanning electron microscopy, transmission electron microscopy, and X-ray diffraction. Electrochemical characterization was performed by cyclic voltammetry and galvanostatic charge–discharge measurements. The results show that $Co(OH)_2$–$Ni(OH)_2$/USY microstructure applied for the electrochemical energy storage has displayed superior capacitive performance. The effect of heat treatment conditions on specific capacitance properties was also systemically explored. Upon annealing at 250 °C, the maximum specific capacitance was up to 479 F/g (or 1,710 F/g after correcting for the weight percent of Co $(OH)_2$–$Ni(OH)_2$ phase). Annealing temperatures higher than 250 °C may cause the hydroxide to form oxide phase and decrease the surface activity of the oxide, thereby leading to a decline of the specific capacitance.

Keywords $Co(OH)_2$–$Ni(OH)_2$ composite · Annealing temperature · Supercapacitors

Y.-Y. Liang · H.-L. Li (✉)
College of Materials Science and Technology of Nanjing University of Aeronautics and Astronautics,
Nanjing 210016, People's Republic of China
e-mail: lihl@lzu.edu.cn

Y.-Y. Liang · S.-J. Bao · H.-L. Li
College of Chemistry and Chemical Engineering of Lanzhou University,
Lanzhou 730000, People's Republic of China

Introduction

Growing environmental concerns and increasing depletion of fossil fuels have created interest in alternative energy technologies. Electrochemical redox capacitors (supercapacitors), which combine the advantages of both dielectric capacitors that can deliver high power within a very small period and rechargeable batteries that store high energy, are becoming attractive energy systems particularly for applications in hybrid electric vehicles, short-term power sources for mobile electronic devices, etc. For example, hybrid systems consisting of batteries and electrochemical capacitors (ECs) are being pursued for electric vehicle propulsion [1, 2]. In such hybrid systems, the ECs can provide the peak power during acceleration, and therefore, the battery can be optimized primarily for higher energy density and better cycle life without the requirement of high power density [3].

Mainly charge-storage mechanisms have been proposed for ECs; notably, double-layer capacitance and charge-transfer-reaction pseudocapacitance. Double-layer capacitance arises from the separation of charge at the interface between a solid electrode and an electroyte [4, 5], whereas pseudocapacitance arises from fast, reversible faradic reactions occurring at or near a solid electrode surface over an appropriate range of potential [6, 7]. As the double-layer capacitance is typically less than 40 $\mu F/cm^2$, most commercially available ECs make use of high-surface-area materials, such as active carbon and carbon fiber, to store energy. However, as much as 90% of the available surface area is not utilized in these materials due to the presence of micropores (<2 nm), which cannot be wetted by the electrolyte.

Transition metal oxides like RuO_2 [6] and IrO_2 [8] exhibit pseudocapacitances that have been reported to be as

high as 760 F/g, which is associated with redox reactions that go beyond the surface and penetrate into the bulk of these materials. Although the noble oxide system gives very high capacitance performance, it has the inherent disadvantage of being both expensive and toxic. Thus, developing alternative electrode materials with improved characteristics and performances is the next logical step.

Recently, nanostructured electrode materials for ECs have attracted great interest, as they show better rates and capabilities than traditional materials. In nanostructured electroactive materials, the pathways for solid-state diffusion within the electrode material are dramatically shorter than the chemically similar bulk material. In addition, larger surface areas in these materials lead to higher current densities during charge and discharge compared to those of conventional electrodes [9, 10]. Thus, these characteristics have significant implications with respect to energy-storage devices based on electrochemically active materials (such as batteries and, especially, ECs) [11–13].

We had reported a series of composite materials on ultrastable Y zeolite (USY) as the novel ECs [14, 15]. In this paper, our strategy is to use a high-surface-area USY zeolite as the template on which a redox-active Co$(OH)_2$−Ni$(OH)_2$ inorganic nanostructure is synthesized through an improved chemical precipitation process. The unique structure of the nanocomposite consists of a loose network-like Co$(OH)_2$−Ni$(OH)_2$ phase, which supplies a convenient pathway for solid-state diffusion of the active ions within the electrode materials, allowing for fast faradic reactions. Electrochemical studies show that the composite electrode has superior capacitive performance, and the maximum specific capacitance is up to 479 F/g [or 1,710 F/g after correcting for the weight percentage of the Co$(OH)_2$−Ni$(OH)_2$ phase], which is considerably comparable to that of hydrated ruthenium oxide in the acid electrolyte. Furthermore, the effect of annealing temperatures on the electrochemical capacitance characteristics has also been systemically explored.

Experimental

USY was prepared by repeated proton exchange of zeolite NaY (LZPCC, Lanzhou, China; Lanet-Y30, Si/Al=2.3, Brunauer–Emmett–Teller surface area=800 m^2/g) with an aqueous solution of NH_4NO_3 at 35 °C for 15 h followed by steaming at 650 °C for 3 h.

A 30-ml aqueous solution of $NH_3{\cdot}H_2O$ (5 ml, 25–28 wt. %) was added dropwise to the mixed aqueous solution of $CoCl_2{\cdot}6H_2O$ and $NiCl_2{\cdot}6H_2O$ (with the same molar ratio of 0.0126 M, 24.79 wt.%). Then, the same weight of USY was subjected to vigorous magnetic stirring until a light green precipitation of Co$(OH)_2$−Ni$(OH)_2$/USY composite was formed. The final pH was slowly adjusted to be around 8.5. The resulting precipitate was filtered using a centrifugal filtration method and washed with distilled water and ethanol several times. The final product was divided into six portions and heated from 100 to 400 °C in air for 3 h [without special denotation, the Co$(OH)_2$−Ni$(OH)_2$/USY sample is referred to annealing at 100 °C in this work].

The working electrodes were prepared according to the method reported in literature [16]. Eighty weight percent of composite powder was mixed with 7.5 wt.% of acetylene black (>99.9%) and 7.5 wt.% of conducting graphite in an agate mortar until a homogeneous black powder was obtained. To this mixture, 5 wt.% of poly(tetrafuoroethylene) dried powder was added with a few drops of ethanol. After brief evaporation drying, the resulting paste was pressed at 5 MPa to nickel gauze with a nickel wire for the electric connection. The electrode assembly was dried for 16 h at 70 °C in air. Each electrode contained 10 mg of redox active material and had a geometric surface area of about 1 cm^2. Electrochemical measurements were carried out using an electrochemical working station (CHI, Chenhua, Shanghai, China) in a half-cell setup configuration at room temperature. A platinum gauze electrode and a saturated calomel electrode served as the counter electrode and the reference electrode, respectively. Cyclic voltammogram (CV) was collected by polarizing the working electrode between −0.10 and 0.60 V in 1 M KOH aqueous solution. Scanning electron microscopy (SEM) (Quanta 200, FEI, Hillsboro, OR, USA) and transmission electron microscopy (TEM) (Hitachi 600, Hitachi, Tokyo, Japan) were employed to examine the morphology of Co$(OH)_2$−Ni$(OH)_2$/USY composite. The crystal structures of the prepared composites were identified by X-ray diffractometer (D/max-2400 Rigaku, Tokyo, Japan) using Cu Kα radiation.

Results and discussion

The morphology of pure USY and the Co$(OH)_2$−Ni$(OH)_2$/USY composite are examined by SEM and TEM. As shown in Fig. 1a, pure USY particles, with an average diameter of about 500 nm, show regular morphology with good dispersion. Comparing Fig. 1a with Fig. 1b reveals a fundamental morphology change taking place on the outer surface of the patent USY particles. The morphology of the composite appears fuzzy in the SEM and TEM images. Higher-magnification SEM images (Fig. 1c,d) further illustrate that a significant amount of network-like phase covers the exterior of the patent USY particles. It is noteworthy that the network-like structure shows anisotropic morphology characteristics and the formation of a loosely packed microstructure in the nanometer scale. The

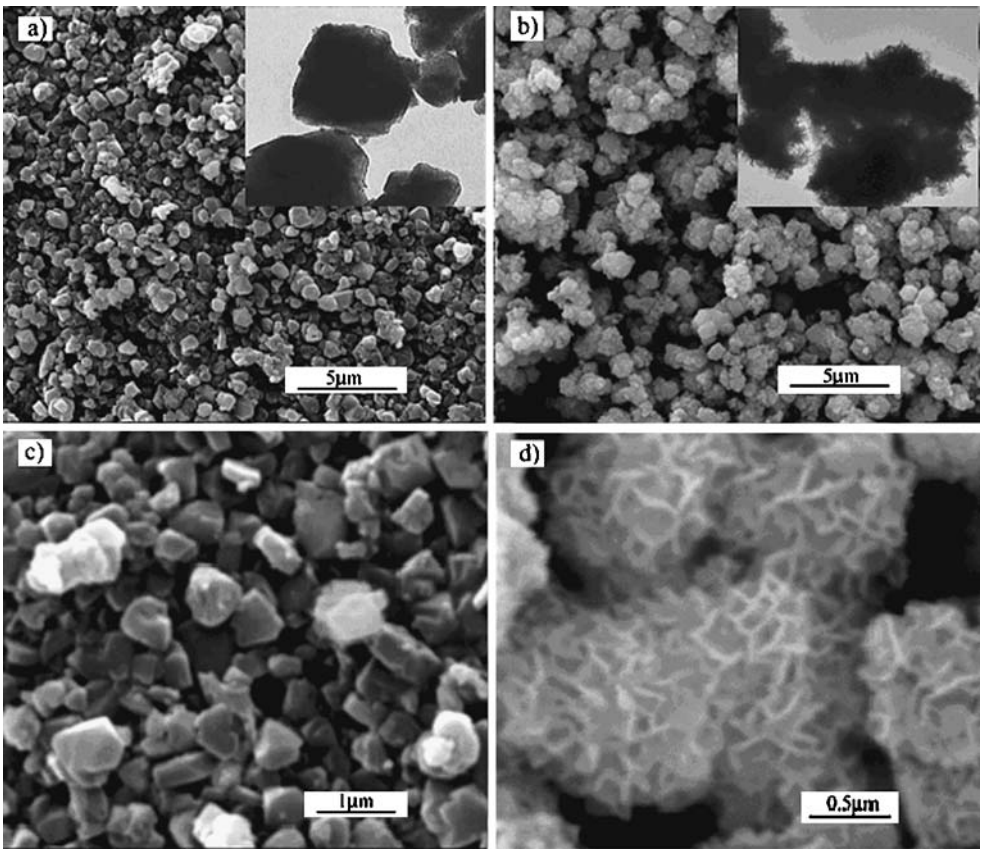

Fig. 1 **a** SEM and TEM images of pure USY; **b** SEM image of $Co(OH)_2$–$Ni(OH)_2$/USY; **c** SEM image of pure USY (higher magnification); **d** SEM image of $Co(OH)_2$–$Ni(OH)_2$/USY (higher magnification)

nanostructure plays a basic role in the morphology requirement for electrochemical accessibility of electrolyte OH^- to $Co(OH)_2$–$Ni(OH)_2$ active material and a fast diffusion rate within the redox phase.

To characterize the crystal phase of $Co(OH)_2$–$Ni(OH)_2$/USY composite material, we employed powder X-ray diffraction (XRD) measurements. As shown in Fig. 2, from curve a corresponding to the pure USY phase, it is noticed that the relatively higher and sharper diffraction peaks have occurred, which are directly linked to good crystallinity or

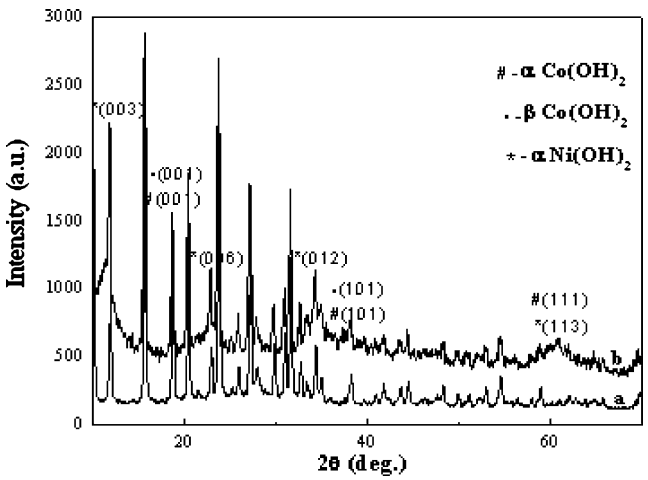

Fig. 2 XRD patterns of **a** pure USY; **b** $Co(OH)_2$–$Ni(OH)_2$/USY

larger crystal grain size. The diffraction patterns of the loaded $Co(OH)_2$–$Ni(OH)_2$ electrochemical active material were corrected by subtracting the reflections of the patent USY phase obtained from curve a. The XRD patterns of loaded $Co(OH)_2$–$Ni(OH)_2$ corresponding to that of pure USY had evidently changed. By contrast, the considerable broadening of diffraction peaks demonstrated that very small crystals of the synthesized $Co(OH)_2$–$Ni(OH)_2$, which correspond to α, β-cobalt hydroxide mixed with nickel in α-type structure. It is well known that cobalt hydroxide is present either in the α phase or in a mixture of α and β phases at room temperature [17].

To understand why the $Co(OH)_2$–$Ni(OH)_2$ phase can grow around the outer surfaces of USY rather than largely forming an isolated phase, it is necessary to first acknowledge some related characteristics of the USY molecular sieve. Negatively charged AlO_4^- tetrahedral units embedded in the structure of USY provide anionic centers for cations to adsorb onto. Proton-exchanged USY absorbs H^+ to keep the charge of the system electronically neutral. During the ion exchange reaction, Co^{2+} and Ni^{2+} ions undergo an exchange with H^+ to balance the negative charge on AlO_4^-. Based on the rule that zeolites preferentially absorb highly charged cations and the fact that USY used in these studies has a low Si/Al ratio [18], it is assumed that a concentration gradient of Co^{2+} and Ni^{2+}

decreasing from the surface of the USY particle gradient towards the solution was created. When pH is increased by NH_4OH titration, $Co(OH)_2$–$Ni(OH)_2$ precipitates will firstly form close to the surface of the USY particles, where Co and Ni ions concentrations are the highest. Sequentially, initial precipitations provide nucleation centers that result in more and more $Co(OH)_2$–$Ni(OH)_2$ buildup extending toward interparticle open space.

To evaluate the microstructure of the prepared $Co(OH)_2$–$Ni(OH)_2$/USY composite and its electrochemical properties, we directly use this composite material to fabricate electrodes for ECs. The applicability of the electrode for ECs was evaluated by CV and galvanostatic charge–discharge measurements. Figure 3 shows CV curves of the composite-based electrode in 1 M KOH as a function of the scan rate in the potential range from −0.1 to 0.6 V. In previous studies [14], it has been demonstrated the pure USY had a negligible integral area under the current-potential response, suggesting that USY alone has very small specific capacitance characteristics. In this case, it is not individually shown in Fig. 3. According to these observations, the $Co(OH)_2$–$Ni(OH)_2$ phases of the composite are responsible for the main capacitance sources. Furthermore, the shape of the CV reveals that the capacitance characteristics of the $Co(OH)_2$–$Ni(OH)_2$ are distinct from those of the electric double-layer systems, with a CV curve close to ideal rectangularship, which is due to faradic reactions of $Co(OH)_2$ and $Ni(OH)_2$ in the potential window, which is shown as follows:

$$Co(OH)_2 + OH^- \leftrightarrow CoOOH + H_2O + e^- \quad (1)$$

$$CoOOH + OH^- \leftrightarrow CoO_2 + H_2O + e^- \quad (2)$$

$$Ni(OH)_2 + OH^- \leftrightarrow NiOOH + H_2O + e^- \quad (3)$$

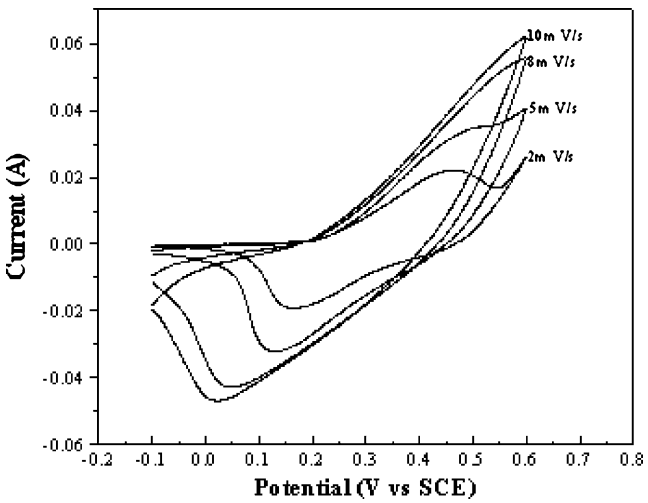

Fig. 3 CVs of $Co(OH)_2$–$Ni(OH)_2$/USY composite electrode at a different scan rate in 1 M KOH within a potential window of −0.1 to 0.45 V

Even though the $Co(OH)_2$–$Ni(OH)_2$/USY material exhibits capacitive behavior, the current-potential response is potential-dependent in contrast to the potential-independent current response of an ideal capacitor. The variation in peak shape with scan rate reflected that the kinetics behavior of faradic reaction that occurred at the electrode/electrolyte interface had more or less changed. An increase in scan rate was correlated with a progressive shift of the cathodic peaks to lower potential, as well as an increase in height. Meanwhile, the relevant anodic peaks have become more and more featureless. A relationship between cathodic current obtained from CV and the scan rate was analyzed shown in Fig. 4. The magnitude of current response in the positive scan was found to be linearly proportional to the square root of the scan rate in the range of 2–10 mV/s (the experimental data are in good accordance with the theoretical evaluation). Such behavior has proved that the charge-storage mechanism of $Co(OH)_2$–$Ni(OH)_2$ is not through a surface redox reaction at the interface but through a diffusion-controlled reaction.

Figure 5 shows the charge–discharge profile of $Co(OH)_2$–$Ni(OH)_2$/USY electrode at different current densities. The corresponding specific capacitance was calculated from

$$C = \frac{I \cdot \Delta t}{\Delta V \cdot M} \quad (1)$$

where M is the mass of the electrode material, ΔV is the potential window, I is the discharge current density, Δt is the total discharge time, and C is the specific capacitance. In this way, the $Co(OH)_2$–$Ni(OH)_2$/USY at a current density of 2 mA/cm^2 exhibited the highest specific capacitance of 367 F/g [or 1,310 F/g after correcting for the weight percentage of the $Co(OH)_2$–$Ni(OH)_2$ phase], which is rather high compared with those of the corresponding hydroxide in the literature [19, 20].

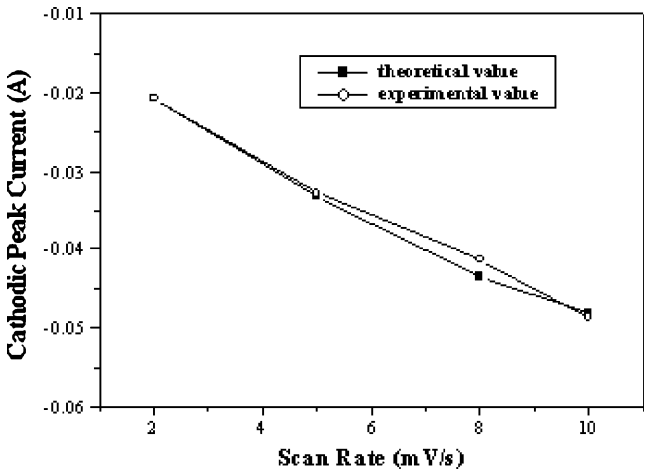

Fig. 4 Effect of the scan rate on the cathodic peak currents obtained from the CV results of the $Co(OH)_2$–$Ni(OH)_2$/USY composite electrode

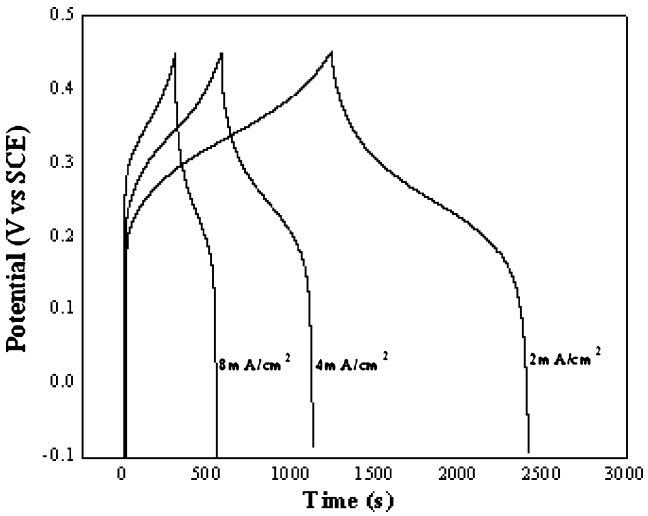

Fig. 5 Charge–discharge behavior of the $Co(OH)_2$–$Ni(OH)_2$/USY composite electrode at different current densities in 1 M KOH within a potential window of −0.1 to 0.45 V

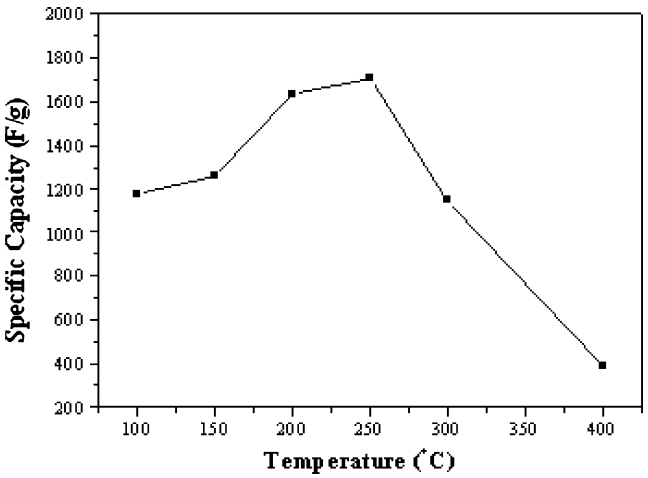

Fig. 7 The real specific capacitance of the $Co(OH)_2$–$Ni(OH)_2$/USY composite electrode [after being corrected for the weight percent of the $Co(OH)_2$–$Ni(OH)_2$ phase] as a function of annealing temperature at the current density of 2 mA/cm^2

Figure 6 shows the specific capacitance of $Co(OH)_2$–$Ni(OH)_2$/USY as a function of the heat-treatment temperature (besides the sample annealing at 100 °C). In the temperature range from 100 to 250 °C, with increasing annealing temperature, the ascending tendency of the specific capacitance is similar and irrelevant to different current densities. The increase in the capacitance characteristic was mainly attributed to the removal of physical and chemical water, which may have opened the pore structure of the composite phase allowing for electrochemical accessibility of electrolyte OH^- to $Co(OH)_2$–$Ni(OH)_2$ active material and a fast diffusion rate within the redox phase, then increasing the specific capacitance performances. Among all these samples, $Co(OH)_2$–$Ni(OH)_2$/USY heated at 250 °C exhibited the maximum specific capacitance of 479 F/g [or 1,710 F/g after correcting for the weight percentage of the Co$(OH)_2$–$Ni(OH)_2$ phase for a single electrode]. When the temperature was higher than 250 °C, the capacitance performances of the $Co(OH)_2$–$Ni(OH)_2$/USY composite were significantly affected by the heat-treatment conditions. Heat treatment was required for thermal decomposition of the nickel and cobalt hydroxide to form oxide phases. Once the oxide phase is formed, further heat-treatment at higher temperature may result in decreased surface area and surface activity of the oxide, thereby leading to a decreased capacitance. Just as in the case of RuO_2, its amorphous phase exhibited far greater specific capacitance than the crystalline counterpart [21].

The real specific capacitance of the $Co(OH)_2$–$Ni(OH)_2$ vs heat-treatment temperature [after correcting the weight percentage of $Co(OH)_2$–$Ni(OH)_2$] is shown in Fig. 7. Although the surface area of $Co(OH)_2$–$Ni(OH)_2$/USY was

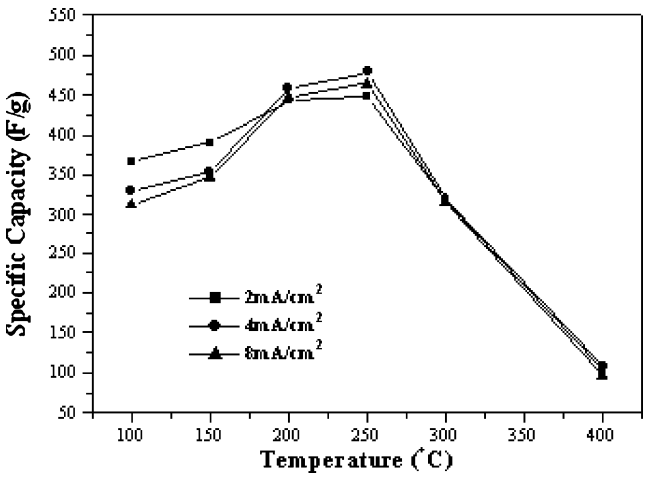

Fig. 6 The specific capacitance of the $Co(OH)_2$–$Ni(OH)_2$/USY composite electrode as a function of annealing temperature with different current densities

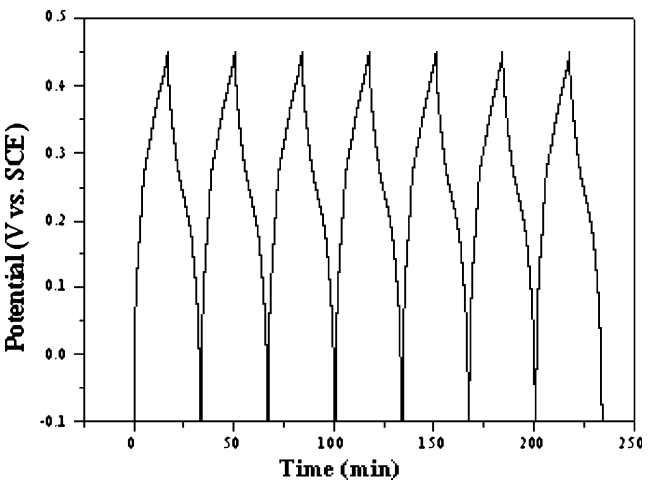

Fig. 8 The first seven charge–discharge cycles of the $Co(OH)_2$–$Ni(OH)_2$/USY composite electrode in 1 M KOH within a potential window of −0.1 to 0.45 V at the current density of 2 mA/cm^2

not measured in this work, a relative comparison of the surface active site of the composite was made in this study. The ratio of the measured capacitance to the total theoretical capacitance of $Co(OH)_2$–$Ni(OH)_2$ is related to the fraction of nickel and cobalt electrochemical active sites, z, involved in the faradic reaction, which can be estimated from the specific capacitance of the composite according to the following equation [22]:

$$z = \frac{C \cdot \Delta V}{F/M} \tag{2}$$

where ΔV is a potential window, 0.55 V in this study; M is an average molecular weight of $Co(OH)_2$–$Ni(OH)_2$, 92.8 g/mol; F is the Faradic constant; and C is the real specific capacitance (F/g). To cite an example, if all the electroactive sites are involved in the faradic reaction, the z value corresponds to 1. The calculation of Eq. 2 gives z value of 0.623, 0.904, and 0.203 at annealing at 100, 250, and 400 °C, respectively. Among these samples, annealing at 250 °C possesses the highest z value of 0.904; in other words, almost more than 90% of the electroactive sites participate in the redox reaction, thus contributing to the maximum specific capacitance of 1,710 F/g.

The considerable high capacitance characteristics and the linearity between the current response and square root of potential scan rate have greatly attracted our attention to detect its unique morphological structure. Assuming that the network-like structure shows anisotropic morphology characteristics provided a convenient pathway for solid-state diffusion of the active ions within the electrode material and enhanced the accessibility of electrolyte OH^- to $Co(OH)_2$–$Ni(OH)_2$ phase, which is contributed to reversibility and bulk accessibility of fast faradic reactions. Thus, we can infer that the USY offers a nanometer template for the formation of network-like $Co(OH)_2$–$Ni(OH)_2$ that is highly dispersed in three-dimensional space. The highly dispersed compound exhibits both a very high surface area and nanoscale microstructure. The superior capacitive performance of the $Co(OH)_2$–$Ni(OH)_2$/USY electrode for ECs is attributed to the high-dispersed capability of USY towards $Co(OH)_2$–$Ni(OH)_2$ phases.

Taking account of the amphiprotic property of zeolite, there is a special importance in examining the electrochemical stability of the composite in 1 M KOH aqueous electrolyte. As is shown in Fig. 8, the specific capacitance loss after 600 consecutive cycles was negligible at about 4%, a fact that proves its excellent long-term electrochemical stability. This experiment indicates that repetitive cycles do not induce noticeable degradation of the microstructure.

Conclusion

In summary, a new strategy to prepare EC materials with very unique microstructures has demonstrated. The novel $Co(OH)_2$–$Ni(OH)_2$/USY nanocomposite was successfully prepared using this strategy. Loosely packed $Co(OH)_2$–$Ni(OH)_2$/USY at the nanometer scale has created electrochemical accessibility of electrolyte OH^- ions and fast diffusion rate through bulk $Co(OH)_2$–$Ni(OH)_2$ at nanometer dimensions, which is very fundamental for electrochemically active materials showing the novel characteristics of supercapacitors rather than conventional batteries. Consequentially, we have achieved the maximum specific capacitance of 479 F/g [or 1,710 F/g after being corrected for the weight percent of the $Co(OH)_2$–$Ni(OH)_2$ phase]. Even though we do not fully understand the fundamental structure of $Co(OH)_2$–$Ni(OH)_2$/USY materials, the strategy reported should be viable to extend to other zeolitic materials and transition metal oxides systems. Work in this direction is being conducted in our lab.

References

1. Burke AF, Murphy TC (1995) Mater Res Soc Symp Proc 393:375
2. Miller J (1995) In: Wolsky SP, Marincic N (eds) Proceedings of the fifth international seminar on double-layer capacitors and similar energy storage devices. Florida Educational Seminars, Boca Raton, FL
3. Jeong YU, Manthiram A (2002) J Electrochem Soc 149:A1419
4. Sarangapani S, Tilak BV, Chen CP (1996) J Electrochem Soc 143:3791
5. Sarangapani S, Lessner P, Forchione J, Griffith A, Laconti AB (1990) J Power Sources 29:355
6. Zheng JP, Cygan PJ, Jow TR (1995) J Electrochem Soc 142:2699
7. Zheng JP, Jow TR (1995) J Electrochem Soc 142:L6
8. Conway BE. In: Delnick FM, Tomkiewicz M (eds) Electrochemical capacitors. PV95-29, p15
9. Sugimoto W, Iwata H, Yasunaga Y, Murakami Y, Takasu Y (2003) Angew Chem Int Ed 42:4092
10. Lee YH, An KH, Kim WS, Park YS, Choi YC, Lee SM, Bea DJ, Lim SC (2001) Adv Mater 13:497
11. Baughman H, Zakhidov AA, de Heer WA (2002) Science 297:787
12. Ghosh S, Inganäs O (1999) Adv Mater 11:1194
13. Zhou YK, Cao L, Zhang FB, He BL, Li HL (2003) J Electrochem Soc 150:A1246
14. Cao L, Xu F, Liang YY, Li HL (2004) Adv Mater 20:1853
15. Cao L, Kong LB, Liang YY, Li HL (2004) Chem Commun 14:1646
16. Toupin M, Brousse T, Belanger D (2002) Chem Mater 14:3946
17. Elumalai P, Vasan HN, Verelst M, Lecante P, Carles V, Tailhades P (2002) Mater Res Bull 37:353
18. Sherry HS (1968) J Colloid Interface Sci 28:288
19. Srinivasan V, Weidner JW (2000) J Electrochem Soc 147:880
20. Lin C, Ritter JA, Popov BN (1998) J Electrochem Soc 145:4097
21. Nan KW, Kim KB (2002) J Electrochem Soc 149:A346
22. Srinivasan V, Weidner JW (2000) J Electrochem Soc 147:880